










## ORIGINAL ARTICLE

OPEN

# Canagliflozin ameliorates the development of NAFLD by preventing NLRP3-mediated pyroptosis through FGF21-ERK1/2 pathway

Shaohan Huang<sup>1</sup>  | Beibei Wu<sup>1</sup>  | Yingzi He<sup>1</sup>  | Ruojun Qiu<sup>1</sup>  |  
 Tian Yang<sup>2</sup>  | Shuo Wang<sup>1</sup>  | Yongzhen Lei<sup>1</sup>  | Hong Li<sup>1</sup>  |  
 Fenping Zheng<sup>1</sup> 

<sup>1</sup>Department of Endocrinology, The Affiliated Sir Run Run Shaw Hospital, School of Medicine, Zhejiang University, Hangzhou, Zhejiang Province, China

<sup>2</sup>Department of Endocrinology, The Affiliated Fourth Hospital, School of Medicine, Zhejiang University, Hangzhou, Zhejiang Province, China

**Correspondence**

Fenping Zheng, Department of Endocrinology, The Affiliated Sir Run Run Shaw Hospital, School of Medicine, Zhejiang University, 3 East Qingchun Road, Hangzhou 310016, Zhejiang Province, China.  
 Email: [3407004@zju.edu.cn](mailto:3407004@zju.edu.cn)

**Abstract**

Recent studies have suggested that sodium-glucose co-transporter2 inhibitors go beyond their glycemic advantages to ameliorate the development of NAFLD. However, little research has been done on the underlying mechanisms. Here, we took deep insight into the effect of canagliflozin (CANA), one of the sodium-glucose co-transporter2 inhibitor, on the progression of NAFLD, and explored the molecular mechanisms. Our findings showed that CANA-treated ob/ob and diabetic mice developed improved glucose and insulin tolerance, although their body weights were comparable or even increased compared with the controls. The CANA treatment ameliorated hepatic steatosis and lipid accumulation of free fatty acid-treated AML12 cells, accompanied by decreased lipogenic gene expression and increased fatty acid  $\beta$  oxidation-related gene expression. Furthermore, inflammation and fibrosis genes decreased in the livers of CANA-treated ob/ob and diabetic mice. FGF21 and its downstream ERK1/2/AMPK signaling decreased, whereas NLRP3-mediated pyroptosis increased in the livers of the ob/ob and diabetic mice, which was reversed by the CANA treatment. In addition, blocking FGF21 or ERK1/2 activity antagonized the effects of CANA on NLRP3-mediated pyroptosis in lipopolysaccharide plus nigericin-treated J774A.1 cells. We conclude that

**Abbreviations:** ACC, acetyl-CoA carboxylase; ACOX1: acyl-coenzyme A oxidase 1; ALP, alkaline phosphatase; ALT, alanine aminotransferase; AST, aspartate aminotransferase; CANA, canagliflozin; CMC-Na, sodium carboxymethyl cellulose solution; CPT1 $\alpha$ , carnitine palmitoyltransferase-1 $\alpha$ ; DM, diabetic mice; ERK1/2, extracellular signal regulated kinase 1 and 2; FASN, fatty acid synthase; FFA, free fatty acids; FGF21, fibroblast growth factor 21; FGFR1, fibroblast growth factor 21 receptor 1; GSDMD, gasdermin D; HFD, high-fat diet; IGPTT, intraperitoneal glucose tolerance test; IR, insulin resistance; ITT, insulin tolerance test; KLB, co-receptor  $\beta$  Klotho; LPS, lipopolysaccharide; MCP-1, monocyte chemoattractant protein-1; NC, normal control; PGC1 $\alpha$ , peroxisome proliferator-activated receptor  $\gamma$  coactivator 1 $\alpha$ ; PI, propidium iodide; PPAR $\alpha$ , peroxisome proliferator-activated receptor  $\alpha$ ; SCD-1, stearoyl-CoA desaturase 1; SGLT-2i, sodium-glucose co-transporter2 inhibitors; SMA, smooth muscle actin; SREBP-1c, sterol regulatory element-binding protein-1c; UALB/CREA, urine albumin to creatinine ratio; T2DM, type 2 diabetes mellitus; WR, wild-type.

Supplemental Digital Content is available for this article. Direct URL citations appear in the printed text and are provided in the HTML and PDF versions of this article on the journal's website, [www.hepcommjournal.com](http://www.hepcommjournal.com)

This is an open access article distributed under the terms of the Creative Commons Attribution-Non Commercial-No Derivatives License 4.0 (CCBY-NC-ND), where it is permissible to download and share the work provided it is properly cited. The work cannot be changed in any way or used commercially without permission from the journal.

Copyright © 2023 The Author(s). Published by Wolters Kluwer Health, Inc. on behalf of the American Association for the Study of Liver Diseases.

CANA treatment alleviated insulin resistance and the progression of NAFLD in ob/ob and diabetic mice independent of the body weight change. CANA protected against the progression of NAFLD by inhibiting NLRP3-mediated pyroptosis and enhancing FGF21-ERK1/2 pathway activity in the liver. These findings suggest the therapeutic potential of sodium-glucose co-transporter2 inhibitors in the treatment of NAFLD.

## INTRODUCTION

Type 2 diabetes mellitus (T2DM) is a contemporary global health issue, and it is closely related to the obesity epidemic. Insulin resistance (IR) and decreased insulin secretion are its core defects, in addition, genetic and environmental variables are linked to T2DM's impaired glucose homeostasis.<sup>[1]</sup> Obesity raises the possibility of getting IR and T2DM. Large amounts of nonesterified fatty acids, proinflammatory cytokines, and other elements released by adipose tissue contribute to the development of IR.<sup>[2]</sup> Furthermore, overflow of excess lipids and inflammatory cytokines due to increased visceral fat mass promotes ectopic lipid deposition and lipotoxicity in the liver and other tissues, eventually contributing to IR.<sup>[3]</sup>

There is a relationship exists between IR and NAFLD, and the prevalence of NAFLD in patients with T2DM is higher than that in patients without T2DM.<sup>[4]</sup> NAFLD often occurs in a broader range of free fatty acid (FFA)-induced metabolic abnormalities that affect the liver and other tissues, as most organs are not suitable for storing large amounts of excess FFAs. Not only due to the accumulation of FFAs but also from inadequate adaptation to toxic lipid-derived metabolites in hepatocyte, activation of various inflammatory pathways, endoplasmic reticulum stress, etc., ultimately leading to apoptosis.<sup>[5]</sup> Although exercise and diet are the cornerstones of NAFLD treatment, medication is urgently needed due to the poor compliance of patients.<sup>[6]</sup> As T2DM and NAFLD are closely related in pathologically and epidemiologically, there are currently no licensed treatments available for NAFLD, which is why antidiabetic drugs are prominent in the detection of suitable medications.<sup>[7]</sup>

Both the novel glucose-lowering medications sodium-glucose cotransporter 2 inhibitors (SGLT-2i) and glucagon-like peptide 1 receptor agonists lead to body weight loss<sup>[8]</sup> and cardiovascular and kidney benefits.<sup>[9]</sup> SGLT2 is highly expressed in the proximal tubule and is responsible for glucose reabsorption,<sup>[10]</sup> typically accounting for ~97% of renal glucose reabsorption under normoglycemic conditions.<sup>[11]</sup> By inhibiting renal glucose reabsorption and promoting glycosuria, SGLT-2i reduces blood glucose in T2DM patients. Clinical studies<sup>[12,13]</sup> have shown that SGLT-2 is such as dapagliflozin and empagliflozin improve

liver steatosis and ameliorate liver enzymes in patients with T2DM and NAFLD, although body weight reduction cannot be excluded. Another population-based large study<sup>[14]</sup> indicated that SGLT-2i has a stronger effect on alleviating serum transaminase levels than glucagon-like peptide 1 receptor agonists in patients with T2DM and NAFLD, even if the weight loss effect is weaker, suggesting that SGLT-2i may have unique mechanisms to attenuate the progression of NAFLD.

Administering SGLT-2i has a beneficial effect on NAFLD even though some animal models have shown no significant effect on body weight.<sup>[15,16]</sup> The potential mechanisms of SGLT-2i on the development of NAFLD include inhibiting hepatic fatty acid synthesis, and alleviating endoplasmic reticulum stress, oxidative stress, inflammation, and so on.<sup>[17]</sup> However, the mechanism by which SGLT-2i-induced benefit in NAFLD have not been fully elucidated.

Fibroblast growth factor 21 (FGF21), a recently identified metabolic regulator, binds to fibroblast growth factor receptor 1 (FGFR1) and the co-factor  $\beta$ -Klotho (KLB) to regulate glucose and lipid metabolism.<sup>[18]</sup> A previous study showed that administering FGF21 and an FGF21 analog reduces liver steatosis in different animal models of NAFLD.<sup>[19]</sup> Indeed, giving a FGF21 analog attenuates the development of hepatic steatosis, inflammation, and fibrosis in the presence of FGF21 deficiency.<sup>[20]</sup> Pyroptosis, a novel variation of programmed cell death, is responsible for cell lysis and proinflammatory cytokines release when triggered by inflammatory stimuli.<sup>[21]</sup> The cleavage of gasdermin D (GSDMD) by the caspase-1 enzyme causes cell membranes to rupture and release intracellular contents, perpetuating the inflammatory cascade.<sup>[22]</sup> NLRP3 inflammasome activation plays a critical role in caspase-1-dependent pyroptosis.<sup>[23]</sup> In NAFLD, apoptosis and necrosis have received significant attention. But other forms of programmed cell death, such as pyroptosis, might potentially be significant in NAFLD.<sup>[24]</sup> Recent research has found that FGF21 regulates pyroptosis in vascular endothelial cells<sup>[25]</sup> and cardiomyocytes.<sup>[26]</sup> However, little has been reported on the effects of SGLT-2i in improving pyroptosis in NAFLD.

Here, by focusing on FGF21 and pyroptosis, we explored the molecular mechanisms of the SGLT-2i canagliflozin (CANA) on the progression of NAFLD.

## MATERIALS AND METHODS

### Experimental animals

Male C57BL/6 mice and male ob/ob mice with mean body weights of 18 to 25 g were bought from Model Animal Research Center of Nanjing University for the investigations. Mice were housed at a constant temperature ( $25 \pm 2^\circ\text{C}$ ) and humidity (40%–60%), with a 12-hour light and 12-hour dark cycle. Appropriate food and water were also provided.

Body weight-matched ob/ob mice ( $n = 16$ ) of 6-week-old were randomly separated into 2 groups. Groups categorized as follows: (1) wild-type group: as controls for ob/ob mice, male wild-type mice were given access to normal chow ( $n = 8$ ). (2) ob/ob+CANA group: CANA (10 mg/kg/d; oral gavage,  $n = 8$ ) was given to ob/ob mice for 14 weeks and fed on normal chow; (3) ob/ob group: 0.5% CMC-Na (same volume of CANA; oral gavage;  $n = 8$ ) was given to ob/ob mice for 14 weeks and fed on normal chow.

Body weight-matched C57BL/6 mice ( $n = 25$ ) of 6-week-old were randomly separated into 2 groups. (1) NC group: mice as normal controls were fed on normal chow ( $n = 5$ ). (2) diabetic mice (DM) mice: C57BL/6 mice were fed a high-fat diet for 4 weeks ( $n = 20$ ), and then mice were given i.p. injections of 50 mg/kg streptozotocin over the course of 3 days to induce diabetes. One week after induction, mice with random blood glucose concentrations  $\geq 11.1$  mmol/L were regarded as having diabetes mellitus. Body weight-matched DM mice with the following names were randomly assigned to 2 groups: (1) DM+CANA group: DM mice were treated with CANA (10 mg/kg/d; oral gavage;  $n = 10$ ) for 11 weeks and fed on high-fat diet. (2) DM group: DM mice were treated with 0.5% CMC-Na (same volume of CANA; oral gavage;  $n = 10$ ) for 11 weeks and fed on high-fat diet. The dose of CANA adopted in this study were referenced on animal studies.<sup>[27,28]</sup>

Every week, the body weights of mice were measured. Mice were separately kept in the metabolic cage chambers with free access to food and water for 24 hours to assess food intake, water intake, and collect urine volumes.

At the end of the study, mice were sacrificed under anesthesia by inhalation of isoflurane, liver tissues and plasma samples were collected and stored at  $-80^\circ\text{C}$  until analysis. All animal experiments were strictly followed the European Parliament's "Directive 2010/63/EU" and approved by the Institutional Animal Research Committee of Sir Run Run Shaw Hospital.

### Cell culture and treatments

AML12, a mouse hepatocellular cell line, was obtained from American Type Culture Collection. In a humidified

incubator at  $37^\circ\text{C}$  with 5%  $\text{CO}_2$ , cells were grown in DMEM/F12 supplemented with 10% fetal bovine serum (SERANA; S-FBS-EU-015),  $0.1 \mu\text{M}$  dexamethasone (D4902; Sigma-Aldrich), insulin-transferrin-selenium (I3146; Sigma-Aldrich) and 1% penicillin-streptomycin. J774A.1, a murine macrophage line, was purchased from the FuHeng Biology. In a humid incubator at  $37^\circ\text{C}$  with 5%  $\text{CO}_2$ , cells were grown in DMEM enriched with 10% fetal bovine serum and 100 IU/L penicillin-streptomycin.

To induce steatosis, 0.75 mM FFA (palmitic acid: oleic acid, 1:2) was applied to AML12 cells for 24 hours at  $37^\circ\text{C}$ . When using inhibitors, AML12 cells were seeded into 6-well plates at a density of  $1 \times 10^5$  cells per well and were incubated overnight. Cells were first treated for 24 hours with 0.75 mM FFA, followed by 24 hours of CANA (40  $\mu\text{M}$ ) treatment in the presence or absence of PD166866 (10  $\mu\text{M}$ ) or PD98059 (5  $\mu\text{M}$ ).

For induction of pyroptosis, the J774A.1 cells were plated 6-well plates. After cultured overnight, cells were primed with lipopolysaccharide (LPS) (1  $\mu\text{g}/\text{mL}$ ) for 6 hours, then stimulated with nigericin (10  $\mu\text{M}$ ) for 1 hour, CANA (10  $\mu\text{M}$ ) was pretreated for another 1 hour before LPS. The groups were named as follows: (1) CANA(–)LPS(–)nigericin(–) group, (2) CANA(–)LPS(+)nigericin(–) group, (3) CANA(–)LPS(+)nigericin(+) group, (4) CANA(+)LPS(+)nigericin(+) group. When using inhibitors, J774A.1 were seeded  $1 \times 10^6$  cells per well into 6-well plates, and the plates were left in the incubator overnight. Cells were pretreated in the presence and absence of MCC950 (10  $\mu\text{M}$ ), PD166866 (10  $\mu\text{M}$ ), PD98059 (5  $\mu\text{M}$ ), or compound C (10  $\mu\text{M}$ ), after which they were primed with LPS (1  $\mu\text{g}/\text{mL}$ ) for 6 hours, followed by nigericin (10  $\mu\text{M}$ ) for 1 hour, and CANA (10  $\mu\text{M}$ ) for another 1 hour before LPS. The dose of LPS and nigericin used in this investigation was based on earlier research.<sup>[29]</sup>

### Nile red staining

As mentioned under cell culture and treatments, FFA was used as a pretreatment for AML12 cells. Following this, PBS was used to wash the cells 3 times. They were then fixed in 4% formaldehyde, washed once more, and stained for 30 minutes with 0.05  $\mu\text{g}/\text{mL}$  Nile red solution (N8440; Solarbio). After that, DAPI was used to stain the cell nuclei, and an electron microscope (Zeiss) was used to capture photographs.

### Hoechst and propidium iodide (PI) staining

As stated in cell culture and treatments section, J774A.1 macrophages were seeded into 12-well plates and then administered LPS and nigericin treatments. After treatment, J774A.1 cells were twice washed in PBS before being incubated for 20 minutes at  $4^\circ\text{C}$  and

in the dark with Hoechst 33342 dye (5  $\mu$ L) and PI (5  $\mu$ L) (C1056; Beyotime Biotechnology). The fluorescent microscope was used to look at the macrophage cells.

## Histologic analyses

Livers sections were cut at a 4  $\mu$ m interval, fixed in 4% paraformaldehyde and embedded in paraffin, and stained with hematoxylin and eosin and Masson. Then, an optical microscope was used to determine the histologic images. Oil Red O (D027-1-1; Nanjing Jiancheng Bioengineering Institute) was used to stain the tissue slices for 5 minutes, after which they underwent 3 PBS washes. Under an optical microscope, the lipid droplets were examined and captured in pictures.

## Quantitative real-time PCR analyses

TRIzol reagent was used to extract the total RNA from cells and fresh frozen liver tissue samples. *Evo M-MLV* RT Premix (AG11706; Accurate Biotechnology) was used for reverse transcription to produce cDNA. Real-time PCR was then carried out with SYBR Green Premix Pro (AG11701; Accurate Biotechnology). Using  $\beta$ -actin as an internal control, the relative mRNA expression was determined using the  $2^{-\Delta\Delta C_t}$  formulae. Table 1 list includes all primer sequences utilized in this investigation.

## Western blotting

RIPA buffer mixed with 100 mM phenylmethanesulfonyl fluoride was used to lyse cell pellets or tissues (FD0100; Fude Biological Technology). With the help of Bicinchoninic acid analysis, total protein concentration was determined (FD2001; Fude Biological Technology). On an SDS-polyacrylamide gel, protein samples were separated, transferred to PVDF membranes, and then incubated with primary antibodies. Antibodies specific for ERK1/2 (4695), p-ERK1/2 (4370), mTOR (2983), p-mTOR (5536), AMPK (5832), p-AMPK (2535), GSDMD (39754), cleaved GSDMD (10137), ASC (67824), IL-1 $\beta$  (12507) were obtained from Cell Signaling Technology. AMPK (ab32047) and pro-caspase-1+p10+p12 (ab179515) were obtained from Abcam. NLRP3 (AG-20B-0014; AdipoGen),  $\beta$ -actin (66009-1-Ig; Proteintech). HRP goat anti-rabbit IgG (AS014; ABclonal). HRP goat anti-mouse IgG (AS003; ABclonal). The protein bands were analyzed using Image J with  $\beta$ -actin as the internal control.

## ELISA statistical analyses

Serum FGF21 levels of mice were detected by double-antibody sandwich ELISA using mouse FGF21 ELISA

Kit (E-EL-M0029c; Elabscience) following the directions provided by the manufacturer. The optical density for each well was determined using a plate reader at 450 nm. The levels of serum insulin of ob/ob mice were detected by double-antibody sandwich ELISA using a wide range mouse insulin immunoassay kit (MS300; EZassay).

## Immunofluorescence

After 20 minutes of immersion in TBS containing 0.2% Triton X-100, the samples were fixed with 4% paraformaldehyde for 20 minutes. They were then blocked with 5% bovine serum albumin and incubated with the primary antibody at 4°C overnight before being incubated with fluorescent-dye-conjugated secondary antibodies. Cell nuclei were stained with DAPI.

## Immunohistochemical analyses

Liver sections were incubated with secondary antibodies after being stained with NLRP3 primary antibodies (G-20B-0014; AdipoGen) at 4°C overnight. After that, sections were stained with diaminobenzidine to produce images of the tissues under a fluorescence microscope (Nikon).

## Transmission electron microscopy examination

J774A.1 cells were prepared as instructed in the section on cell culture and treatments, washed in PBS, and collected using a plastic cell scraper. After being centrifugation at 2000 rpm for 5 minutes to form pellets, the cells were fixed in ice-cold 2.5% glutaraldehyde for 2 hours. The samples were then dehydrated and embedded in epoxy resin after being post-fixed in 1% OsO<sub>4</sub> for an hour. Finally, transmission electron microscopy analysis of ultrathin sections double-stained with uranyl acetate and lead citrate (Tecnai, T10, Holland).

## Statistical analyses

GraphPad Prism 8 was used to analyze the values in this study. All results are displayed as the mean  $\pm$  SD. The comparisons between the 2 groups were made using unpaired Student *t* tests. Differences between several groups were analyzed using 1-way ANOVA. A *p*-value < 0.05 was considered statistically significant (\**p* < 0.05, \*\**p* < 0.01, \*\*\**p* < 0.001).

**Table 1** Primer sequences

Genes	Forward	Reverse
Primers for quantitative real-time PCR analysis		
SREBP-1c	CAGACTCACTGCTGCTGACA	GATGGTCCCTCCACTCACCA
FASN	GGCCCCCTCTGTTAATTGGCT	GGATCTCAGGGTTGGGGTTG
SCD-1	GTACCGCTGGCACATCAACT	AACTCAGAAGCCCAAAGCTCA
ACC	GCCTCAGGAGGATTTGCTGT	AGGATCTACCCAGGCCACAT
PPAR $\alpha$	TGCCTTCCCTGTGAAGTAC	TGGGGAGAGAGGACAGATGG
CPT1 $\alpha$	GGACTCCGCTCGCTCATT	GAGATCGATGCCATCAGGGG
NLRP3	ATTACCCGCCCGAGAAAGG	CATGAGTGTGGCTAGATCCAAG
Caspase-1	AATACAACCACTCGTACACGTG	AGCTCCAACCCTCGGAGAAA
IL-1 $\beta$	GAAATGCCACCTTTTGACAGTG	TGGATGCTCTCATCAGGACAG
IL-18	GCCTGTGTTTCGAGGATATGACT	CCTTCACAGAGAGGGTCACAG
GSDMD	TTCAGGCCCTACTGCCTTCT	GTTGACACATGAATAACGGGGTT
ASC	GACAGTGCAACTGCGAGAAG	CGACTCCAGATAGTAGCTGACAA
Col1a1	CGCCATCAAGGTCTACTGC	ACGGGAATCCATCGGTCA
Col1a2	CCGTGCTTCTCAGAACATCA	CTTGCCCCATTCAATTTGTCT
SMA	AAGAGCATCCGACACTGCTGAC	AGCACAGCCTGAATAGCCACATAC
$\beta$ -actin	AGGCCAACCGTGAAAAGATG	AGAGCATAGCCCTCGTAGATGG
Primers for PCR analysis		
FGF21	TCTGAACCTGACCCATCCCT	GTACCTCTGCCGGACTTGAC
FGFR1	TACACCTGCATCGTGAGAAT	GTCGGTGCGGAGATCGTTC
KLB	AGGGTCTCCGGGGAATGAAT	GCTGACTTGGGTTTACCGGA

Abbreviations: ACC, acetyl-CoA carboxylase; CPT1 $\alpha$ , carnitine palmitoyltransferase-1 $\alpha$ ; FASN, fatty acid synthase; FGF21, fibroblast growth factor 21; FGFR1, fibroblast growth factor 21 receptor 1; GSDMD, gasdermin D; KLB, co-receptor  $\beta$  Klotho; PPAR $\alpha$ , peroxisome proliferator-activated receptor  $\alpha$ ; SCD-1, stearoyl-CoA desaturase 1; SMA, smooth muscle actin; SREBP-1c, sterol regulatory element-binding protein-1c.

## RESULTS

### Canagliflozin treatment improves the metabolic phenotype and insulin sensitivity

Figure 1 is the study design. As expected, ob/ob mice treated with CANA consumed more food and water and urinated more than control ob/ob mice; however, body weights were comparable between the 2 groups (Figures 2A–C, H). The CANA treatment increased food intake in the DM mice, accompanied by more body weight gain (Figures 2D–F, I). In the ob/ob and DM mice, CANA therapy restored normal fasting blood glucose levels (Figures 2J, K). The lower glucose AUC on IPGTT indicated increased glucose tolerance in ob/ob and DM mice treated with CANA (Figures 2L, M). In addition, the CANA-treated ob/ob and DM mice had increased insulin sensitivity, as seen by decreased fasting serum insulin levels in the ob/ob mice and glucose AUC of ITT in the DM mice (Figures 2N, O). In addition, CANA-treated DM mice had a significantly lower urine albumin-creatinine ratio compared with the DM control mice (Figure 2G).

### Canagliflozin alleviates lipid droplet accumulation in the liver and FFA-induced AML12 cells and improves liver function, inflammation, and fibrosis

Representative livers of ob/ob and DM mice were greasy and whiter than those of the CANA-treated mice (Figures 3A, C). The CANA treatment decreased liver weight in the DM mice and ob/ob mice (Figures 3B, D). The CANA treatment significantly attenuated liver steatosis and hepatocyte ballooning in the ob/ob and DM mice, as detected by Oil Red O staining and hematoxylin and eosin (Figures 3E–H). In addition, plasma levels of alanine aminotransferase, aspartate aminotransferase, and alkaline phosphatase were decreased significantly in the CANA-treated ob/ob and DM mice (Figures 3I, J).

Then, CANA's cytotoxicity was examined by treating mouse AML12 cells with 0, 20, 40, 60, 80, and 100  $\mu$ M for 24 hours (Figure 3K). Cell viability was decreased with increasing CANA dose over 40  $\mu$ M. The effect of 40  $\mu$ M CANA on lipogenesis was further confirmed in the FFA-induced steatotic AML12 cells by Nile red staining (Figure 3L).



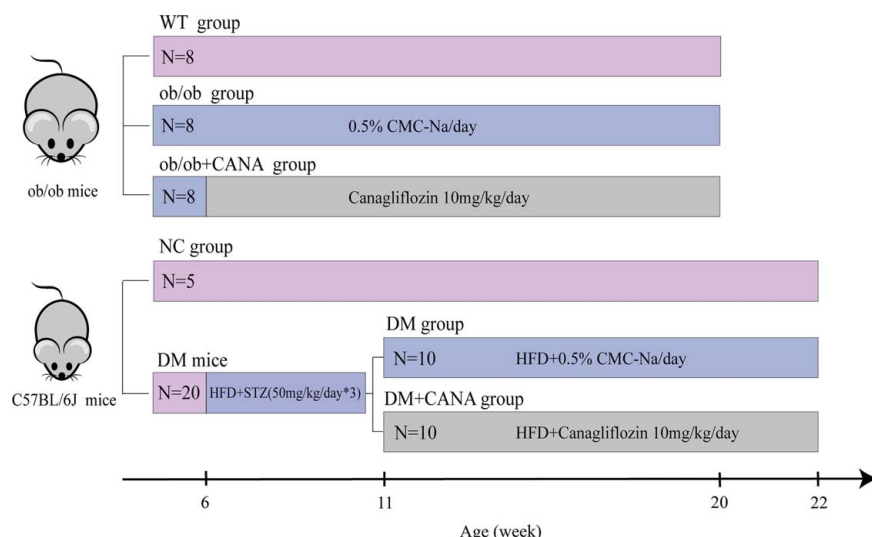


**Figure 1** Study design. Body weight-matched ob/ob mice ( $n = 16$ ) in 6-week-old were randomly assigned, into 2 groups (each with 8 mice). (1) Wild-type group: 8 male wild-type mice were fed on normal chow. (2) ob/ob+CANA group: CANA (10 mg/kg/d; oral gavage,  $n = 8$ ) was given to ob/ob mice for 14 weeks and fed, on normal chow. (3) ob/ob group: 0.5% CMC-Na (same volume of CANA; oral gavage;  $n = 8$ ) was given to, ob/ob mice for 14 weeks and fed on normal chow. Body weight-matched C57BL/6 mice ( $n = 25$ ) were randomly divided into 2 groups. (1) NC group: 5 mice as normal controls fed on normal chow. (2) DM mice: another 20 more C57BL/6 mice were fed a HFD for 4 weeks, and then mice were given i.p. injections of 50 mg/kg streptozotocin over the course of 3 days to induce diabetes. Body weight-matched DM mice were randomly divided into 2 groups. (1) DM+CANA group: DM mice treated with CANA (10 mg/kg/d; oral gavage;  $n = 10$ ) for 11 weeks and fed on HFD. (2) DM group: DM mice treated with, 0.5% CMC-Na (same volume of CANA; oral gavage;  $n = 10$ ) for 11 weeks and fed on HFD. Abbreviations: CANA, canagliflozin; CMC-Na, sodium carboxymethyl cellulose solution; DM, diabetes mice; HFD, high-fat diet; NC, normal control; STZ, streptozotocin; WT, wild-type.

Consistent with the alleviated lipid accumulation, genes related to lipogenesis, including sterol regulatory element-binding protein-1c (SREBP-1c) and acetyl-CoA carboxylase, were significantly downregulated, whereas genes of fatty acid  $\beta$ -oxidation, including peroxisome proliferator-activated receptor alpha (PPAR $\alpha$ ), acyl-coenzyme A oxidase 1, and peroxisome proliferator-activated receptor  $\gamma$  coactivator 1 $\alpha$  were significantly upregulated in the livers of the CANA-treated ob/ob and DM mice (Figures 4A, B, D, E). Furthermore, the expression levels of inflammatory factors, TNF- $\alpha$ , and monocyte chemoattractant protein-1 were decreased markedly, as were the expression levels of fibrotic factors, including col1a1 and col1a2 in the livers of ob/ob and DM mice treated with CANA (Figures 4C, F). Liver fibrosis was confirmed by Masson staining (Figures 4G, H), showing that the collagen-deposited area was significantly smaller in the livers of the ob/ob and DM mice treated with CANA.

### Canagliflozin improves the FGF21 signaling pathway in the liver and AML12 cells

To further explore the molecular mechanisms of improved NALFD by SGLT-2i, transcriptomic analysis of liver samples was performed to identify differential gene expression profiles. The KEGG pathway analysis showed that the “PPAR signaling pathway” (KEGG

No. 3320) was the most relevant in the ob/ob and DM mice (Figures 5A, B). The key PPAR  $\alpha$ -regulated hepatokine is FGF21, which acts during fasting, starvation, and a ketogenic diet, to encourage fatty acid  $\beta$  oxidation and ketogenesis in the liver and reduce liver and body lipids.<sup>[30]</sup> Therefore, the hepatic mRNA and serum levels of FGF21, as well as FGF21, FGFR1, and KLB mRNAs were assessed. FGF21, FGFR1, and KLB mRNAs were significantly induced in the liver of DM mice after the CANA treatment, accompanied by elevated serum FGF21 levels (Figures 5E, F). When ob/ob mice were treated with CANA, it was interesting to see that either the liver FGF21 mRNA expression or the serum levels of FGF21 decreased, whereas FGFR1 expression rose (Figures 5C, D), indicating greater FGF21 sensitivity in the liver of ob/ob mice.

The major FGF21 signaling pathway in the regulation of hepatic energy metabolism includes ERK1/2, AMPK, and mTOR<sup>[31]</sup>; thus, the liver's ERK1/2/AMPK/mTOR signaling activity were evaluated. Increased ERK1/2 activity was detected after the CANA treatment in the ob/ob and DM mice. Moreover, increased mTOR or AMPK activity was found in the liver of the CANA-treated ob/ob mice and DM mice, respectively (Figures 5G, H). Consistently, ERK1/2 and AMPK activity were increased in response to the CANA treatment in FFA-induced steatotic mouse AML12 cells, and which was abrogated by pretreatment with the FGFR1 inhibitor PD166866 or the ERK1/2 inhibitor PD98059 (Figures 5I–K).

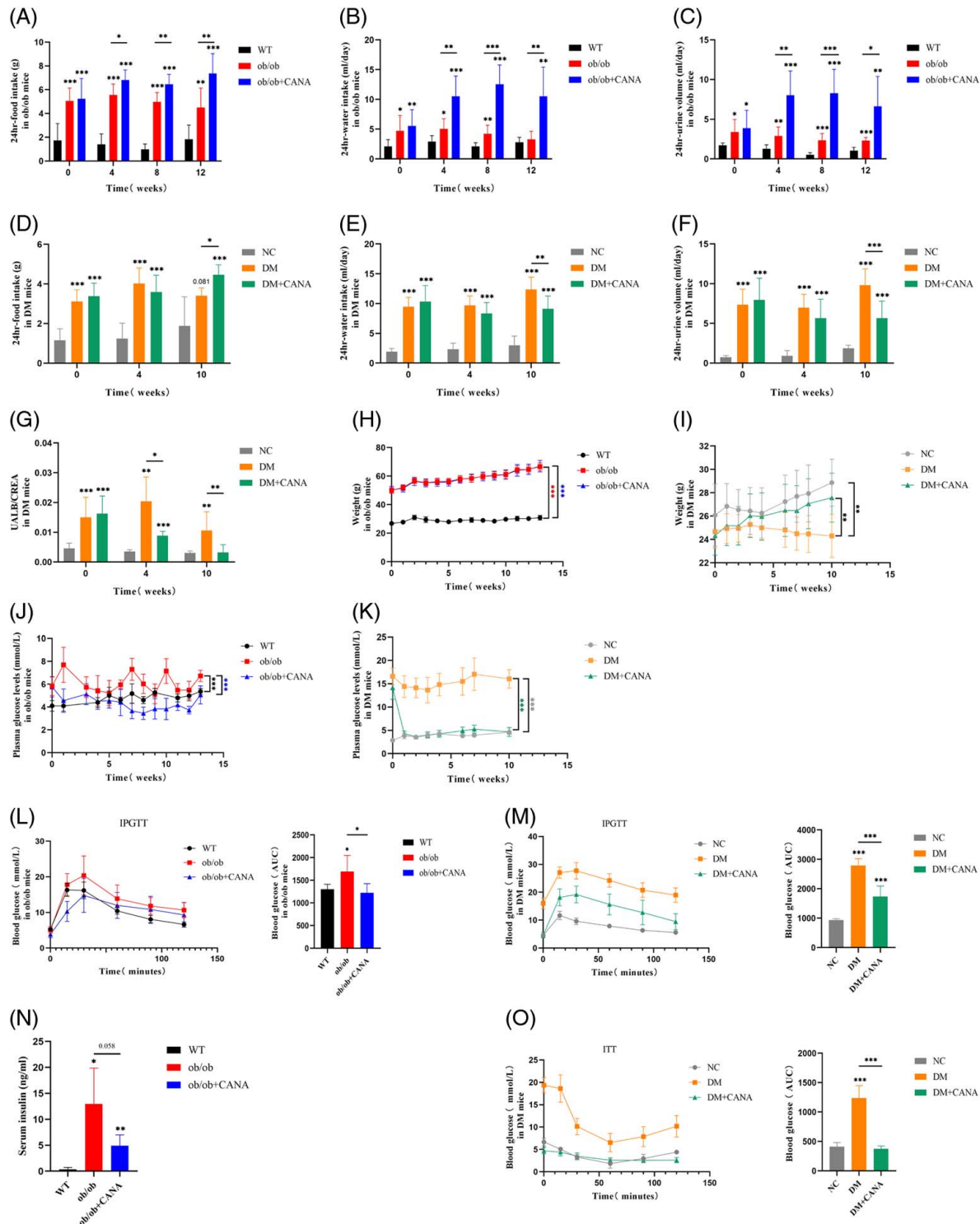


**Figure 2** Effects of CANA on metabolism phenotype and insulin resistance. Both ob/ob and DM mice were treated as mentioned in the Materials and Methods section. Mice were kept in metabolic cages to record food intake (A, D), water intake (B, E), urine volume (C, F), and UALB/CREA ratio (G) during CANA treatment. (H and I) Body weight change in response to 16-week and 11-week CANA treatment in ob/ob and DM mice, respectively. (J and K) Fasting plasma glucose level. (L and M) Blood glucose levels and AUC during IPGTT in 8-week CANA treatment ob/ob mice and 10-week CANA treatment DM mice. (N) Fasting serum insulin levels of ob/ob mice assessed by ELISA. (O) Blood glucose levels and AUC during ITT in DM mice receiving 10-week CANA treatment. Data are presented as mean  $\pm$  SD ( $n = 4-8$  in ob/ob mice,  $n = 5-10$  in DM mice). \* $p < 0.05$ ; \*\* $p < 0.01$ ; \*\*\* $p < 0.001$ . Abbreviations: CANA, canagliflozin; DM, diabetes mice; IPGTT, intraperitoneal glucose tolerance test; ITT, insulin tolerance test; NC, normal control; UALB/CREA, urine albumin to creatinine ratio; WT, wild-type.

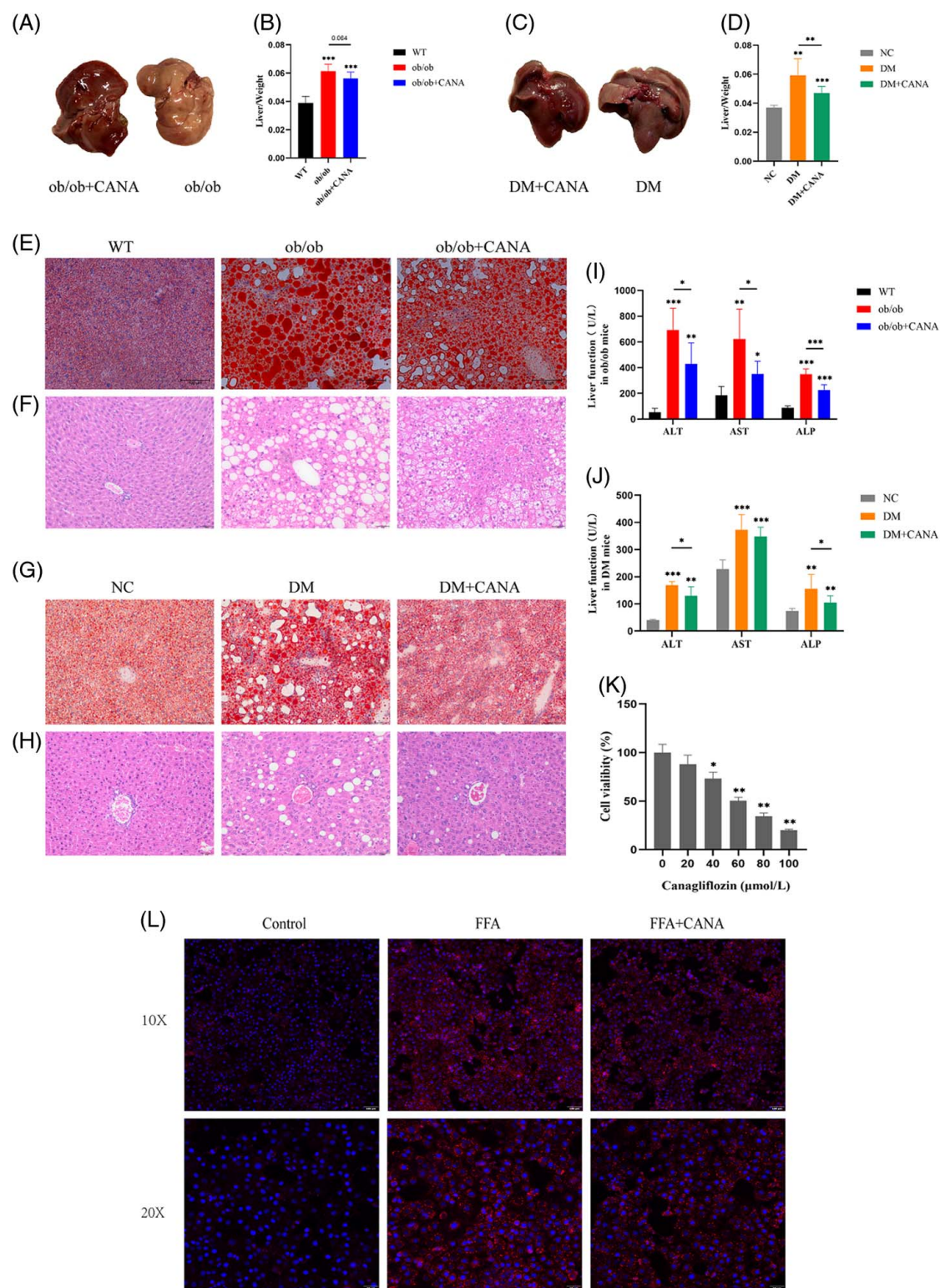


**Figure 3** Effects of CANA on lipid droplets accumulation and liver function in mice. Representative images of external liver appearance (A, C) and liver/body weight ratio (B, D) after CANA treatment in the ob/ob and DM mice, respectively. Representative images of Oil Red O staining (E, G) and hematoxylin and eosin staining (F, H) of liver sections. (I and J) Liver function evaluated by ALT, AST, and ALP levels. Data are presented as mean  $\pm$ SD ( $n = 4-8$  in ob/ob mice,  $n = 5-10$  in DM mice).  $*p < 0.05$ ;  $**p < 0.01$ ;  $***p < 0.001$ . (K) Cell viability levels of AML12 cells after 0, 20, 40, 60, 80, and 100  $\mu$ M CANA extract for 24 hours. Data are presented as mean  $\pm$ SD.  $*p < 0.05$ ;  $**p < 0.01$ . (L) Graphical representation of, changes in Nile red staining in FFA-induced steatotic mouse AML12 cells. Abbreviations: ALP, alkaline phosphatase; ALT, alanine aminotransferase; AST, aspartate amino-transferase; CANA, canagliflozin; DM, diabetic mice; FFA, free fatty acids; NC, normal control; WT, wild-type.



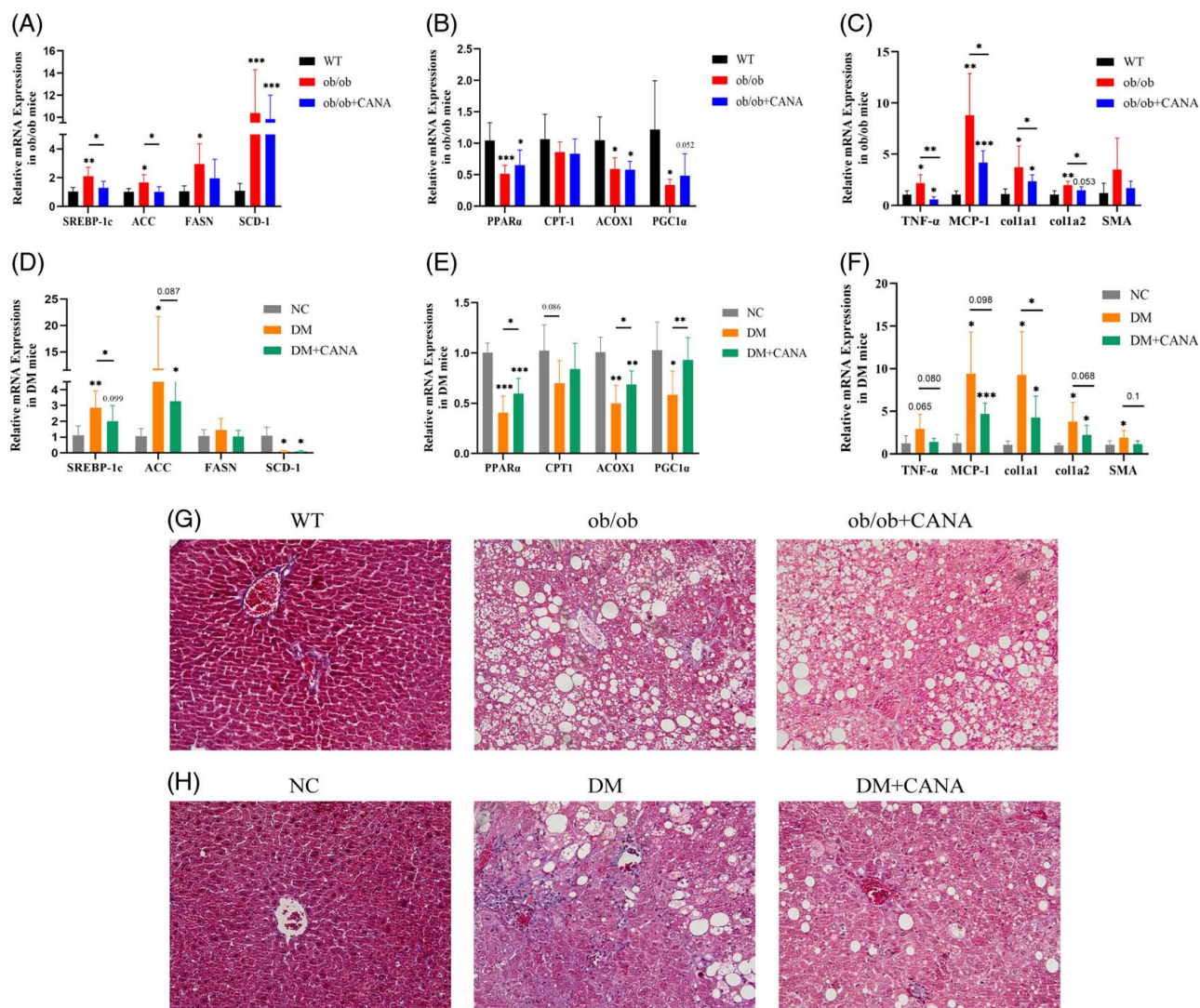


**Figure 4** Related gene expressions of liver lipogenesis, fatty acid  $\beta$ -oxidation, inflammation, and fibrosis. Hepatic mRNA expression of lipogenesis (A, D), fatty acid  $\beta$ -oxidation (B, E), inflammation and fibrosis, genes in the ob/ob and DM mice (C, F). Representative images of Masson staining of liver tissue sections (G, H). Data are presented as mean  $\pm$  SD ( $n=4-8$  in ob/ob mice,  $n=5-10$  in DM mice). \* $p < 0.05$ ; \*\* $p < 0.01$ ; \*\*\* $p < 0.001$ . Abbreviations: ACC, acetyl-CoA carboxylase; ACOX1: acyl-coenzyme A oxidase 1; CANA, canagliflozin; CPT1 $\alpha$ , carnitine palmitoyltransferase-1 $\alpha$ ; DM, diabetic mice; FASN, fatty acid synthase; MCP-1, monocyte chemoattractant protein-1; PGC1 $\alpha$ , peroxisome proliferator-activated receptor  $\gamma$  coactivator 1 $\alpha$ ; PPAR $\alpha$ , peroxisome proliferator-activated receptor  $\alpha$ ; SCD-1, stearoyl-CoA desaturase 1; SMA, smooth muscle actin; SREBP-1c, sterol regulatory element-binding protein-1c; WT, wild-type.

### Canagliflozin ameliorates NLRP3-related pyroptosis in the liver and J774A.1 cells treated with LPS and nigericin

Since NLRP3-mediated pyroptosis is a key factor in the development of NAFLD<sup>[32,33]</sup> and FGF21 has anti-inflammatory properties, the levels of NLRP3 expression were examined in the livers of mice given CANA. NLRP3, which is mainly expressed in hepatocytes and macrophages, was slightly increased in the livers of ob/ob mice but significantly increased in DM mice, which was reversed by the CANA treatment in DM mice (Figures 6A, B). In addition, pyroptosis-related protein levels of cleaved caspase-1 (p10), cleaved GSDMD, ASC, and IL-1 $\beta$  were also markedly

decreased in CANA-treated DM mice. Whereas, only decreased cleaved GSDMD levels and IL-1 $\beta$  were found in the livers of CANA-treated ob/ob mice (Figures 6C–F).

To investigate the effect of CANA on pyroptosis, LPS in combination with nigericin was used to induce pyroptosis in J774A.1 cells. First, cytotoxicity of CANA was examined by treating J774A.1 cells with 0, 5, 10, 20, 50, 100, and 200  $\mu$ M for 24 hours (Figure 7A). Cell viability was decreased with increasing CANA dose over 10  $\mu$ M. Second, transmission electron microscopy revealed irregular outlines of the cells, and holes in the cell membranes and rupture of the cell surface were visible in the LPS plus nigericin-treated cells. In addition, the nuclei were karyopyknotic and the

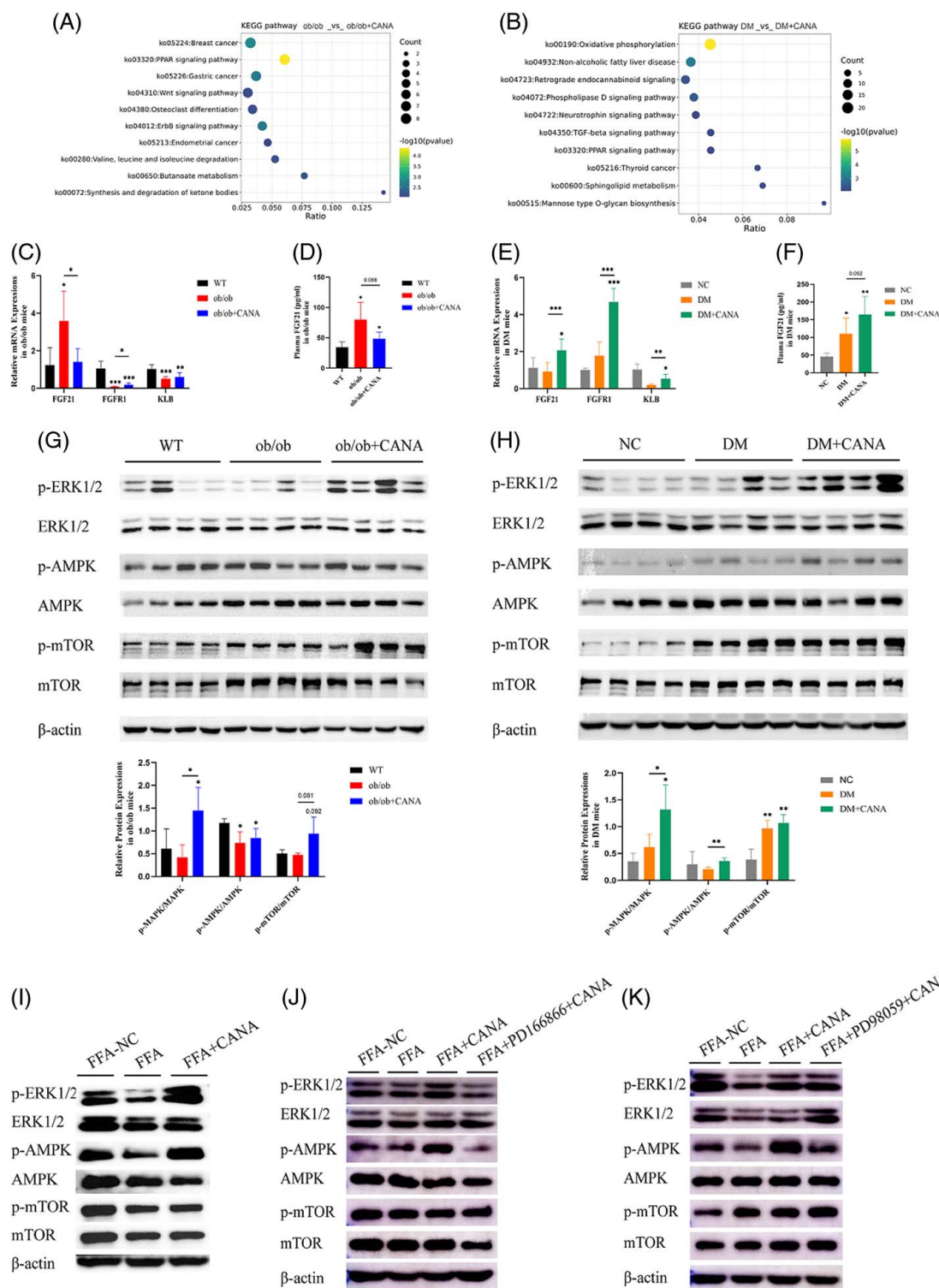


**Figure 5** Effects of CANA on FGF21 signaling pathway in the liver and AML12 cells. (A and B) KEGG, pathway enrichment analysis of targets of different gene expression that were related to CANA-treated, ob/ob mice, and DM mice. (C and E) Expression of KLB, FGFR1, and FGF21 mRNA in the livers. (D and F) Serum, FGF21 levels were measured by ELISA in ob/ob ( $n = 4-8$ ) and DM mice ( $n = 5-10$ ). Representative western blot of ERK1/2, p-ERK1/2, AMPK, p-AMPK, mTOR and p-mTOR in the livers (G, H). FFA (0.75 mM) was, applied to AML12 cells for 24 hours in both the absence and presence of CANA (40  $\mu$ M), PD166866 (10  $\mu$ M) or, PD98059 (5  $\mu$ M). (I-K) Representative western blot of ERK1/2, AMPK, and mTOR. Data are presented as mean  $\pm$  SD. \* $p < 0.05$ ; \*\* $p < 0.01$ ; \*\*\* $p < 0.001$ . Abbreviations: CANA, canagliflozin; DM, diabetic mice; FFA, free fatty acids; FGF21, fibroblast growth factor 21; FGFR1, fibroblast growth factor 21 receptor 1; KLB, co-receptor  $\beta$  Klotho; NC, normal control; WT, wild-type.



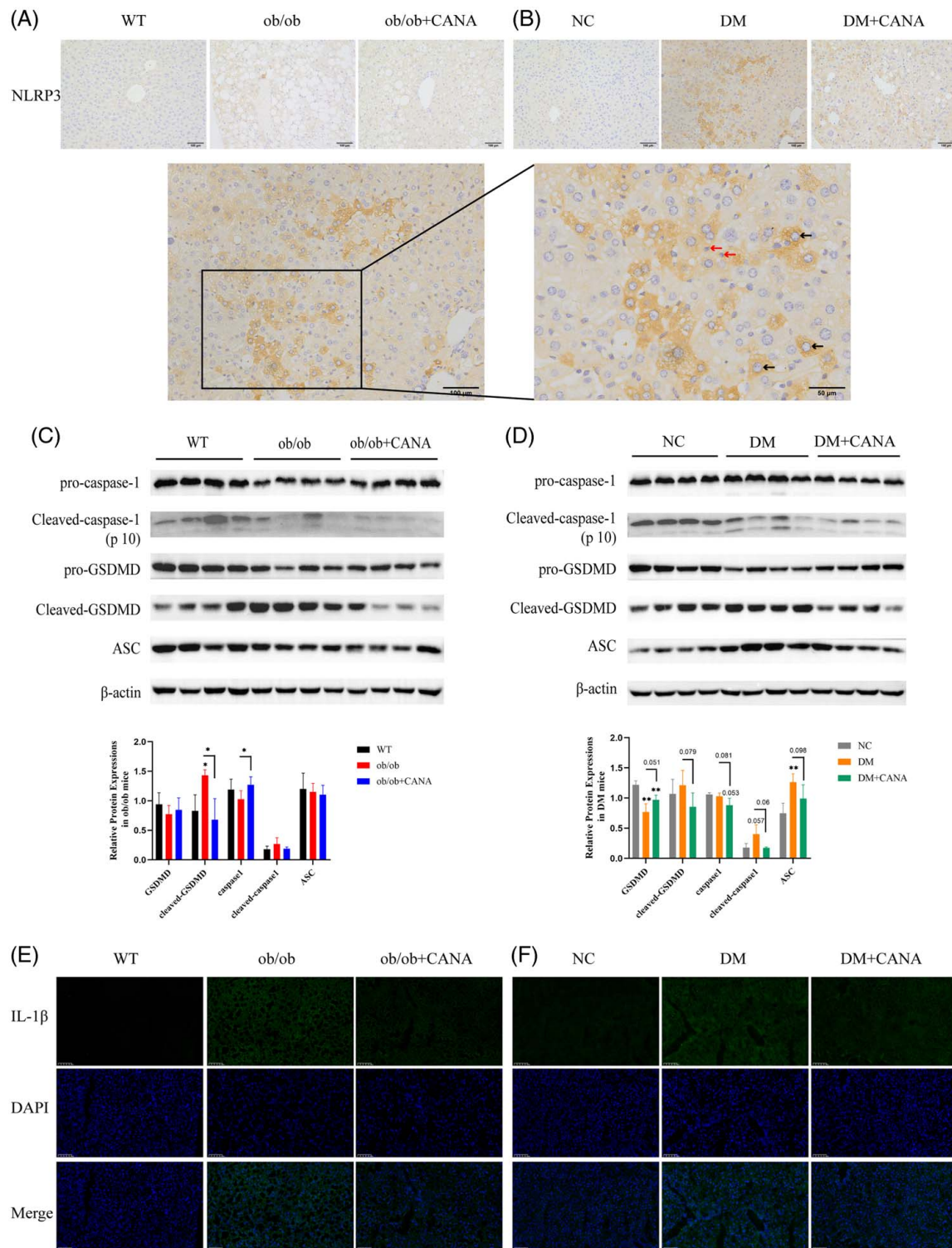


**Figure 6** Effects of CANA on NLRP3-related pyroptosis in the livers of ob/ob and DM mice. (A and B) Representative images of immuno-histochemical staining for NLRP3 in mouse liver sections. Examples of NLRP3-positive hepatocytes (black arrows) and macrophages (red arrows). (C and D) Pyroptosis-related proteins, in liver tissues, including pro-caspase-1, cleaved-caspase-1, pro-GSDMD, cleaved GSDMD, and ASC, were examined by western blot. (E and F) Immunofluorescence analysis of IL-1 $\beta$  (green). Abbreviations: CANA, canagliflozin; DM, diabetic mice; GSDMD, gasdermin D; NC, normal control; WT, wild-type.

cytoplasm contained several cytoplasmic organelles with many large vacuoles. However, cell morphology was improved after supplementation with CANA of 10  $\mu$ M (Figure 7B). In addition, cell death was observed

(PI stain) in J774A.1 cells treated with LPS and nigericin (Figure 7C).

In the LPS plus nigericin-treated J774A.1 cells (Figures 7D–F), increased expression of NLRP3,

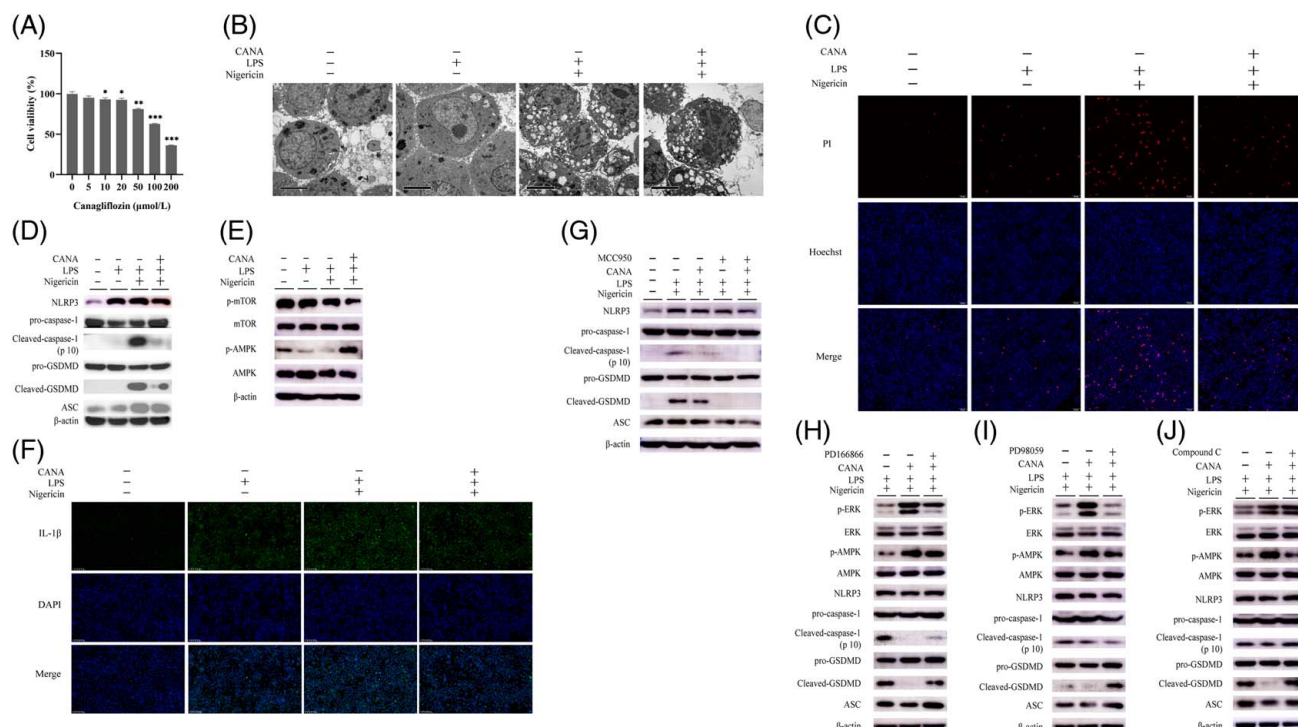


**Figure 7** Effects of CANA on NLRP3-related pyroptosis in J774A.1 cells treated with LPS and nigericin. (A) Cell viability levels of J774A.1 cells after 0, 5, 10, 20, 50, 100, and 200  $\mu$ M CANA extract for 24 hours. Transmission electron microscopic images (B) and PI staining images. NLRP3, caspase-1, GSDMD (C), and ASC (D) protein expression levels of in J774A.1 cells. (E) Representative western blot of AMPK, p-AMPK, mTOR, and p-mTOR. (F) Immunofluorescence analysis of IL-1 $\beta$  (green) in J774A.1 cells. (G) Representative, western blot of NLRP3, caspase-1, GSDMD, and ASC in J774A.1 cells treated with LPS+nigericin, MCC950, and CANA. (H–J) NLRP3, caspase-1, GSDMD, and ASC in J774A cells from various treatment groups are, shown in this representative western blot. The cells were pretreated in the absence or presence of, PD166866 (10  $\mu$ M), PD98059 (5  $\mu$ M), and compound C (10  $\mu$ M) for 1 hour, then treated for 6 hours with LPS, 1 hour for nigericin, and another 1 hour with CANA (10  $\mu$ M) before LPS. Data are presented as mean  $\pm$  SD. \* $p$  < 0.05; \*\* $p$  < 0.01; \*\*\* $p$  < 0.001. Abbreviations: CANA, canagliflozin; GSDMD, gasdermin D; LPS, lipopolysaccharide; PI, propidium iodide.

cleaved-caspase-1 (p10), cleaved-GSDMD, ASC, and IL-1 $\beta$ , as well as decreased AMPK and mTOR activity were found, which were all reversed by pretreatment of CANA 10  $\mu$ M. Like CANA, one of the NLRP3-selective inhibitors MCC950 showed comparable inhibition on NLRP3, cleaved-caspase-1 (p10), cleaved GSDMD and ASC, and CANA and MCC950 had additive effects on them (Figure 7G).

### Canagliflozin ameliorates pyroptosis through the FGF21 signaling pathway in J774A.1 cells treated with LPS and nigericin

Both J774A.1 cells and AML12 cells had expressions of FGF21 and its receptors, FGFR1 and KLB (Supplemental Figure 1, <http://links.lww.com/HC9/A101>). To further explore the role of FGF21 signaling activity mediating the effect of CANA on NLRP3-mediated pyroptosis, blockers of FGF21 signaling were induced in LPS plus nigericin-induced J774A.1 cells. CANA decreased the pyroptosis-related proteins of NLRP3, cleaved-caspase-1, cleaved GSDMD, and ASC, while increasing p-ERK1/2 and p-AMPK in LPS plus

nigericin-induced J774A.1 cells. However, the effects of CANA on all of them were diminished by pretreatment with the FGFR1 inhibitor PD166866 or the ERK1/2 inhibitor PD98059 (Figures 7H, I). Although compound C did not antagonize the effect of CANA on p-ERK1/2 (Figure 7J), it also antagonized CANA's effects on NLRP3-related pyroptosis. These results indicated that CANA activated FGF21-ERK1/2-AMPK signaling, thus inhibiting the NLRP3-related pyroptosis pathway.

## DISCUSSION

The most prevalent liver disease in the world is NAFLD, which is on the rise, yet the available treatments are still insufficient.<sup>[34]</sup> The 3 main pathogenic causes of NAFLD are T2DM, obesity, and hyperlipidemia.<sup>[35]</sup> SGLT-2i has an anti-hyperglycemic effect by enhancing urinary glucose excretion.<sup>[36]</sup> In addition to its apparent role in glycemic control, SGLT-2i has been previously demonstrated in human studies and different animal models for its therapeutic potential for NAFLD.<sup>[37]</sup> However, the underlying mechanism by which SGLT-2i has its action besides glycosuria is not fully understood yet. Our study revealed that the CANA treatment alleviated IR, liver



steatosis, inflammation, and fibrosis in the ob/ob and DM mice independent of body weight loss. The protective effect of SGLT-2i against NAFLD progression was mainly due to the enhanced action of FGF21 in the liver and its mediating effect on inhibiting NLRP3-associated pyroptosis.

NAFLD was recognized as a long-term positive energy balance disorder caused by hypercaloric diet and a sedentary lifestyle.<sup>[38]</sup> Previous studies showed that the magnitude of weight reduction appears to be positively correlated with the improvements in liver histologic activity.<sup>[39]</sup> Interestingly, according to recent studies, body mass index or weight loss is not necessary to reduce liver fat content or to restore normal liver function.<sup>[40]</sup> SGLT-2i results in a significant loss of urine glucose in patients taking SGLT-2i by reducing glucose reabsorption. Over time, cumulative calorie loss can lead to significant weight loss.<sup>[41]</sup> However, the protective effect of SGLT-2i against the development of NAFLD is not absolutely connected to weight loss, as our data did not demonstrate that CANA decreased body weight in either ob/ob or DM mice. Growing evidence for the effect of SGLT-2i treatment on body weight is inconsistent, as some studies have reported weight loss,<sup>[42]</sup> stable weight,<sup>[16]</sup> or weight gain.<sup>[43]</sup> In line with a prior study that claimed that the SGLT-2 inhibitor dapagliflozin induces sustained glucose excretion into urine and compensatory hyperphagia attenuates SGLT-2i-induced weight loss,<sup>[44]</sup> no changes in body weight of CANA-treated ob/ob mice was most likely due to the increased energy intake (food intake, water intake, or both) compensating for the loss of urinary glucose. The high expenditure with hyperglycemia in the DM mice was alleviated by CANA therapy, leading to gradual body weight gain. Consistently, our findings suggest that SGLT-2i affected NAFLD regardless of the discrepancy in the body weight change. In this work, we found that CANA administration can improve IR and lower blood glucose levels in ob/ob and DM mice, which may contribute to the alleviation of NAFLD. But at least the protection of CANA against NAFLD is independent of body weight. Furthermore, these observations in different animal models imply that SGLT-2i may be a viable therapeutic medication for the treatment of NAFLD.

IR is closely related to the development of NAFLD.<sup>[4]</sup> In this study, we observed that the CANA treatment improved insulin sensitivity despite no loss of body weight. The KEGG pathway analysis focused on the PPAR signaling pathway. PPAR $\alpha$  is highly expressed in hepatocytes and it regulates many aspects of hepatic lipid metabolism.<sup>[45]</sup> FGF21 is a hepatokine induced by activation of PPAR $\alpha$  during fasting or a ketogenic diet. Previous studies have shown that the PPAR $\alpha$ -FGF21 pathway modulates energy balance or affects NAFLD-related pathways.<sup>[46,47]</sup> Recent studies demonstrated that SGLT-2i activates catabolic pathways, reduces

hepatic steatosis, and increases hepatic and plasma levels of FGF21.<sup>[42]</sup> Our data show that improved FGF21 sensitivity and action in the liver may have contributed to the improvement of IR and the progression of NAFLD by CANA.

As reported,<sup>[48]</sup> circulating FGF21 was elevated in ob/ob mice, indicating FGF21 resistance in an obese state. By contrast, peripheral FGF21 was low in DM mice, suggesting a deficiency of FGF21 activity. However, the CANA treatment increased FGF21 activity by increasing hepatic FGF receptor expression as well as downstream phosphorylation of the ERK1/2-AMPK pathway, accompanied by decreased and increased circulating FGF21 levels in ob/ob and DM mice, respectively. Therefore, it was exciting that CANA ameliorated the FGF21-resistant state in obesity,<sup>[49]</sup> and raises the promise that SGLT-2i can be applied to NAFLD target FGF21 activity, although the mechanism needs further investigation.

It is becoming more and more clear that pyroptosis and the development of NAFLD are closely related.<sup>[24]</sup> Pyroptosis occurs when the NLRP3 inflammasome is activated,<sup>[33]</sup> and GSDMD acts as an executor through its caspase-cleaved GSDMD-N domain (cleaved GSDMD), triggering pyroptosis and leading to the release of IL-1 $\beta$ .<sup>[50]</sup> We discovered that NLRP3-mediated pyroptosis existed in the ob/ob and DM mice, supporting their relationship. This is the first report that suggests CANA may improve NAFLD by alleviating pyroptosis, to the best of our knowledge. FGF21 has been found to regulate pyroptosis.<sup>[25,26]</sup> We recognized that CANA alleviated NLRP3-mediated pyroptosis by increasing FGF21 activity as shown in our animal studies, as either an FGFR1 blocker or inhibiting ERK1/2 diminished the inhibitory effect of CANA on pyroptosis in LPS plus nigericin-induced J774A.1 cells. There is no research on FGF21's impact on pyroptosis in the liver. However, FGF21 could decrease pyroptosis in vascular endothelial cells<sup>[25]</sup> and cardiomyocytes.<sup>[26]</sup> Given the critical role of pyroptosis in the development of NAFLD,<sup>[24]</sup> our study provides a biological basis for SGLT-2i treatment in NAFLD. However, the underlying SGLT-2i molecular mechanism of enhancing FGF21 activity in the liver (eg, SGLT-2 or SGLT-1 dependent, SGLT independent or secondary to ketone bodies) remains to be explored.

Taken together, our results demonstrate that CANA has a favorable impact on the progression of NAFLD by improving insulin sensitivity, liver steatosis, inflammation, and fibrosis in obese and DM animal models. The protective effect of CANA occurred mainly by alleviating NLRP3-mediated pyroptosis and increasing FGF21 activity in the liver. Our study provides insight into applying SGLT-2i to the treatment of NAFLD.

## AUTHOR CONTRIBUTIONS

Shaohan Huang and Beibei Wu performed the experiments, collected the data, and prepared the manuscript.

Yingzi He, Ruojun Qiu, Shuo Wang, and Tian Yang performed partial experiments and analyzed the data. Yongzhen Lei and Hong Li contributed to revision of manuscript. Fenping Zheng designed the experiments, revise, and edit the manuscript. The final version of the manuscript was approved by all authors.

## FUNDING INFORMATION

Supported by the Bethune Charitable Foundation (B0307H20200302); National Natural Science Foundation of China (81870583); Medical Science and Technology Project of Zhejiang Province (2011KYB159).

## CONFLICT OF INTEREST

The authors declare no conflicts of interest.

## ORCID

Shaohan Huang <https://orcid.org/0000-0002-8979-1317>

Beibei Wu <https://orcid.org/0000-0002-6404-7997>

Yingzi He <https://orcid.org/0000-0001-5730-4388>

Ruojun Qiu <https://orcid.org/0000-0002-5496-0352>

Tian Yang <https://orcid.org/0000-0002-8085-1838>

Shuo Wang <https://orcid.org/0000-0001-9601-3436>

Yongzhen Lei <https://orcid.org/0000-0002-5820-3199>

Hong Li <https://orcid.org/0000-0003-4158-1860>

Fenping Zheng <https://orcid.org/0000-0002-1091-2367>

## REFERENCES

- DeFronzo RA, Ferrannini E, Groop L, Henry RR, Herman WH, Holst JJ, et al. Type 2 diabetes mellitus. *Nat Rev Dis Primers*. 2015;1:15019.
- Kahn SE, Hull RL, Utzschneider KM. Mechanisms linking obesity to insulin resistance and type 2 diabetes. *Nature*. 2006;444:840–6.
- Abildgaard J, Danielsen ER, Dorph E, Thomsen C, Juul A, Ewertsen C, et al. Ectopic lipid deposition is associated with insulin resistance in postmenopausal women. *J Clin Endocrinol Metab*. 2018;103:3394–404.
- Fujii H, Kawada N. Japan Study Group of NAFLD (JSG-NAFLD). The role of insulin resistance and diabetes in nonalcoholic fatty liver disease. *Int J Mol Sci*. 2020;21:3863.
- Cusi K. Role of insulin resistance and lipotoxicity in non-alcoholic steatohepatitis. *Clin Liver Dis*. 2009;13:545–63.
- Vilar-Gomez E, Martinez-Perez Y, Calzadilla-Bertot L, Torres-Gonzalez A, Gra-Oramas B, Gonzalez-Fabian L, et al. Weight loss through lifestyle modification significantly reduces features of nonalcoholic steatohepatitis. *Gastroenterology*. 2015;149:367–78.e5; quiz e14–5.
- Dewidar B, Kahl S, Pafili K, Roden M. Metabolic liver disease in diabetes—from mechanisms to clinical trials. *Metabolism*. 2020;111s:154299.
- Patoulas D, Stavropoulos K, Imprialos K, Katsimardou A, Kalogirou MS, Koutsampasopoulos K, et al. Glycemic efficacy and safety of glucagon-like peptide-1 receptor agonist on top of sodium-glucose co-transporter-2 inhibitor treatment compared to sodium-glucose co-transporter-2 inhibitor alone: a systematic review and meta-analysis of randomized controlled trials. *Diabetes Res Clin Pract*. 2019;158:107927.
- Nelson AJ, Pagidipati NJ, Aroda VR, Cavender MA, Green JB, Lopes RD, et al. Incorporating SGLT2i and GLP-1RA for cardiovascular and kidney disease risk reduction: call for action to the Cardiology Community. *Circulation*. 2021;144:74–84.
- Vallon V, Platt KA, Cunard R, Schroth J, Whaley J, Thomson SC, et al. SGLT2 mediates glucose reabsorption in the early proximal tubule. *J Am Soc Nephrol*. 2011;22:104–12.
- Gorboulev V, Schürmann A, Vallon V, Kipp H, Jaschke A, Klessen D, et al. Na(+)-D-glucose cotransporter SGLT1 is pivotal for intestinal glucose absorption and glucose-dependent incretin secretion. *Diabetes*. 2012;61:187–96.
- Shimizu M, Suzuki K, Kato K, Jojima T, Iijima T, Murohisa T, et al. Evaluation of the effects of dapagliflozin, a sodium-glucose co-transporter-2 inhibitor, on hepatic steatosis and fibrosis using transient elastography in patients with type 2 diabetes and non-alcoholic fatty liver disease. *Diabetes Obes Metab*. 2019;21:285–92.
- Kuchay MS, Krishan S, Mishra SK, Farooqui KJ, Singh MK, Wasir JS, et al. Effect of empagliflozin on liver fat in patients with type 2 diabetes and nonalcoholic fatty liver disease: a randomized controlled trial (E-LIFT Trial). *Diabetes Care*. 2018;41:1801–8.
- Pradhan R, Yin H, Yu O, Azoulay L. Glucagon-like peptide 1 receptor agonists and sodium-glucose cotransporter 2 inhibitors and risk of nonalcoholic fatty liver disease among patients with type 2 diabetes. *Diabetes Care*. 2022;45:819–29.
- Hüttel M, Markova I, Miklankova D, Zapletalova I, Poruba M, Haluzik M, et al. In a prediabetic model, empagliflozin improves hepatic lipid metabolism independently of obesity and before onset of hyperglycemia. *Int J Mol Sci*. 2021;22:11513.
- Steven S, Oelze M, Hanf A, Kröller-Schön S, Kashani F, Roohani S, et al. The SGLT2 inhibitor empagliflozin improves the primary diabetic complications in ZDF rats. *Redox Biol*. 2017;13:370–85.
- Androutsakos T, Nasiri-Ansari N, Bakasis AD, Kyrou I, Efsthopoulos E, Randeva HS, et al. SGLT-2 Inhibitors in NAFLD: Expanding Their Role beyond Diabetes and Cardioprotection. *Int J Mol Sci*. 2022;23:3107.
- Fisher FM, Maratos-Flier E. Understanding the physiology of FGF21. *Annu Rev Physiol*. 2016;78:223–41.
- Keinicke H, Sun G, Mentzel CMJ, Fredholm M, John LM, Andersen B, et al. FGF21 regulates hepatic metabolic pathways to improve steatosis and inflammation. *Endocr Connect*. 2020;9:755–68.
- Zarei M, Pizarro-Delgado J, Barroso E, Palomer X, Vázquez-Carrera M. Targeting FGF21 for the treatment of nonalcoholic steatohepatitis. *Trends Pharmacol Sci*. 2020;41:199–208.
- Qiu T, Pei P, Yao X, Jiang L, Wei S, Wang Z, et al. Taurine attenuates arsenic-induced pyroptosis and nonalcoholic steatohepatitis by inhibiting the autophagic-inflammasomal pathway. *Cell Death Dis*. 2018;9:946.
- Lamkanfi M, Dixit VM. Manipulation of host cell death pathways during microbial infections. *Cell Host Microbe*. 2010;8:44–54.
- Sun L, Ma W, Gao W, Xing Y, Chen L, Xia Z, et al. Propofol directly induces caspase-1-dependent macrophage pyroptosis through the NLRP3-ASC inflammasome. *Cell Death Dis*. 2019;10:542.
- Beier JI, Banales JM. Pyroptosis: An inflammatory link between NAFLD and NASH with potential therapeutic implications. *J Hepatol*. 2018;68:643–5.
- Zeng Z, Zheng Q, Chen J, Tan X, Li Q, Ding L, et al. FGF21 mitigates atherosclerosis via inhibition of NLRP3 inflammasome-mediated vascular endothelial cells pyroptosis. *Exp Cell Res*. 2020;393:112108.
- Chen JJ, Tao J, Zhang XL, Xia LZ, Zeng JF, Zhang H, et al. Inhibition of the ox-LDL-induced pyroptosis by FGF21 of human umbilical vein endothelial cells through the TET2-UQCRC1-ROS pathway. *DNA Cell Biol*. 2020;39:661–70.
- Nasiri-Ansari N, Dimitriadis GK, Agogiannis G, Perrea D, Kostakis ID, Kaltsas G, et al. Canagliflozin attenuates the progression of atherosclerosis and inflammation process in APOE knockout mice. *Cardiovasc Diabetol*. 2018;17:106.

28. Hira T, Koga T, Sasaki K, Hara H. Canagliflozin potentiates GLP-1 secretion and lowers the peak of GIP secretion in rats fed a high-fat high-sucrose diet. *Biochem Biophys Res Commun.* 2017;492:161–5.
29. Zhang C, Zhao C, Chen X, Tao R, Wang S, Meng G, et al. Induction of ASC pyroptosis requires gasdermin D or caspase-1/11-dependent mediators and IFN $\beta$  from pyroptotic macrophages. *Cell Death Dis.* 2020;11:470.
30. Lu W, Li X, Luo Y. FGF21 in obesity and cancer: new insights. *Cancer Lett.* 2021;499:5–13.
31. Rebollo-Hernanz M, Aguilera Y, Martin-Cabrejas MA, Gonzalez de Mejia E. Phytochemicals from the cocoa shell modulate mitochondrial function, lipid and glucose metabolism in hepatocytes via activation of FGF21/ERK, AKT, and mTOR pathways. *Antioxidants (Basel).* 2022;11:136.
32. Thomas H. NAFLD: a critical role for the NLRP3 inflammasome in NASH. *Nat Rev Gastroenterol Hepatol.* 2017;14:197.
33. Gaul S, Leszczynska A, Alegre F, Kaufmann B, Johnson CD, Adams LA, et al. Hepatocyte pyroptosis and release of inflammasome particles induce stellate cell activation and liver fibrosis. *J Hepatol.* 2021;74:156–67.
34. Liu Y, Wang DW, Wang D, Duan BH, Kuang HY. Exenatide attenuates non-alcoholic steatohepatitis by inhibiting the pyroptosis signaling pathway. *Front Endocrinol.* 2021;12:663039.
35. Younossi ZM, Loomba R, Rinella ME, Bugianesi E, Marchesini G, Neuschwander-Tetri BA, et al. Current and future therapeutic regimens for nonalcoholic fatty liver disease and nonalcoholic steatohepatitis. *Hepatology.* 2018;68:361–71.
36. Gallo LA, Wright EM, Vallon V. Probing SGLT2 as a therapeutic target for diabetes: basic physiology and consequences. *Diab Vasc Dis Res.* 2015;12:78–89.
37. Petito-da-Silva TI, Souza-Mello V, Barbosa-da-Silva S. Empagliflozin mitigates NAFLD in high-fat-fed mice by alleviating insulin resistance, lipogenesis and ER stress. *Mol Cell Endocrinol.* 2019;498:110539.
38. Younossi Z, Anstee QM, Marietti M, Hardy T, Henry L, Eslam M, et al. Global burden of NAFLD and NASH: trends, predictions, risk factors and prevention. *Nat Rev Gastroenterol Hepatol.* 2018;15:11–20.
39. Anstee QM, Targher G, Day CP. Progression of NAFLD to diabetes mellitus, cardiovascular disease or cirrhosis. *Nat Rev Gastroenterol Hepatol.* 2013;10:330–44.
40. Worm N. Beyond body weight-loss: dietary strategies targeting intrahepatic fat in NAFLD. *Nutrients.* 2020;12:1316.
41. Tahrani AA, Barnett AH, Bailey CJ. SGLT inhibitors in management of diabetes. *Lancet Diab Endocrinol.* 2013;1:140–51.
42. Osataphan S, Macchi C, Singhal G, Chimene-Weiss J, Sales V, Kozuka C, et al. SGLT2 inhibition reprograms systemic metabolism via FGF21-dependent and -independent mechanisms. *JCI Insight.* 2019;4:e123130.
43. Boland BB, Brown C Jr, Boland ML, Cann J, Sulikowski M, Hansen G, et al. Pancreatic  $\beta$ -cell rest replenishes insulin secretory capacity and attenuates diabetes in an extreme model of obese type 2 diabetes. *Diabetes* 2019;68:131–40.
44. Devenny JJ, Godonis HE, Harvey SJ, Rooney S, Cullen MJ, Pellemounter MA. Weight loss induced by chronic dapagliflozin treatment is attenuated by compensatory hyperphagia in diet-induced obese (DIO) rats. *Obesity (Silver Spring).* 2012;20:1645–52.
45. Kersten S. Integrated physiology and systems biology of PPAR $\alpha$ . *Mol Metab.* 2014;3:354–71.
46. Sun W, Nie T, Li K, Wu W, Long Q, Feng T, et al. Hepatic CPT1A facilitates liver-adipose cross-talk via induction of FGF21 in mice. *Diabetes.* 2021;70:2337/2021-0363.
47. Samuel VT, Shulman GI. Nonalcoholic fatty liver disease as a nexus of metabolic and hepatic diseases. *Cell Metab.* 2018;27:22–41.
48. Hale C, Chen MM, Stanislaus S, Chinookoswong N, Hager T, Wang M, et al. Lack of overt FGF21 resistance in two mouse models of obesity and insulin resistance. *Endocrinology.* 2012;153:69–80.
49. Fisher FM, Chui PC, Antonellis PJ, Bina HA, Kharitonov A, Flier JS, et al. Obesity is a fibroblast growth factor 21 (FGF21)-resistant state. *Diabetes.* 2010;59:2781–9.
50. Shi J, Zhao Y, Wang K, Shi X, Wang Y, Huang H, et al. Cleavage of GSDMD by inflammatory caspases determines pyroptotic cell death. *Nature.* 2015;526:660–5.

**How to cite this article:** Huang S, Wu B, He Y, Qiu R, Yang T, Wang S, et al. Canagliflozin ameliorates the development of NAFLD by preventing NLRP3-mediated pyroptosis through FGF21-ERK1/2 pathway. *Hepatol Commun.* 2023;7:e0045. <https://doi.org/10.1097/HC9.0000000000000045>